Proceedings of the 4th Workshop on Quantum Chaos and Localisation Phenomena, Warsaw 2009

Doorway Mechanism in Many-Body Systems and in Quantum Billiards

T. Guhr

Fachbereich Physik, Universität Duisburg-Essen, Lotharstrasse 1, 47057 Duisburg, Germany

Among the numerous different ways to excite many-body and other complex quantum systems, mechanisms are often found which are clearly distinguished by a simple, typically semiclassical interpretation. In nuclei, these are the collective excitations in which all or large groups of particles move coherently. They often act as “doorways” to other excitations of single-particle character. Examples for and the limitations of the doorway mechanism are discussed. Recent results show that superscars in the barrier billiard serve as perfect object to shed light on aspects of the doorway mechanism which are not directly accessible in traditional quantum systems. To this end, two new statistical observables are employed. Some open questions are addressed.

PACS numbers: 05.45.Mt, 03.65.Sq, 24.30.Cz, 21.10.Pc

1. Introduction

The most beautiful feature of statistical physics is its ability to provide a unifying understanding for at first sight different physical phenomena. This enables a fruitful transfer of ideas, insights and approaches. Here, a recent example will be presented. In quantum many--body systems, the variety of possible states is so rich that excitation modes which are somehow “distinct” are indispensable to structure the spectral information obtained in an experiment. By “distinct” we mean excitations which allow for a simple, typically semiclassical, interpretation. Collective excitations in which all particles or large groups of particles move in a spatially coherent fashion [1] are of particular interest. In the sequel, we will discuss examples from nuclear physics. Such a dynamical coherence implies that the motion of the many-body system takes place in a low-dimensional subspace of the full phase space. This in turn makes it possible to describe these excitations by models comprising only very few degrees of freedom. The successful identification of the corresponding states in the spectra yields fundamental information about the dynamics of the system as a whole.

It is, however, highly unlikely that all properties of the collective excitation are fully caught by the low--dimensional model. Put differently, the states resulting from this simplifying model are hardly ever eigenstates of the true many-body Hamiltonian. Of course, if the model is meaningful, they have to be a good approximation for true eigenstates. Hence, the states of the simplifying model have a non-vanishing overlap with the true eigenstates of the system. This leads to the concept of a doorway state: one models the true Hamiltonian of the system as consisting of, first, the simplifying model for the collective states, second, a background of other non-collective states and, third, the coupling between these two classes of states. The non-collective states have single-particle character. Their detailed features are not important to understand the collective motion. Often, not always, one can assume that their number is very large, and one models them statistically. The collective states act via the coupling as “doorways” to the background of the non-collective states [1–3]. Thus, the doorways spread over the background.

Everything which has been said so far is not only valid for collective excitations, it can as well apply to states which are distinct for another reason. A good example is anticrossing spectroscopy in molecular physics, see Ref. [4]. As shown in Fig. 1, a singlet state $|s\rangle$ is excited by a laser from the singlet ground state $|s0\rangle$. This state is not really an eigenstate of the Hamiltonian, because there is a small interaction V_μ with the triplet state $|t\mu\rangle$ which becomes important when the two states are energetically close. The whole manifold of triplet states can be shifted in energy by a strong magnetic field while the singlet states do not change their energetic position. Hence, whenever a triplet state is close to $|s\rangle$, the fluorescence yield from $|s\rangle$ back to $|s0\rangle$ is lowered due to the coupling V_μ. The singlet state acts as a doorway to all these triplet states, rendering precise spectroscopy possible. Further examples for the doorway mechanism can be found in metal clusters, see Refs. [5, 6].

Recently, a full-fledged investigation of the doorway mechanism was presented in Ref. [7]. Certain distinct states, referred to as superscars, in a pseudointegrable microwave billiard were studied by means of new observables which at present cannot be extracted from experimental data in many-body systems. The purpose of this contribution is to discuss these findings and to put them into a proper perspective by relating them to collective

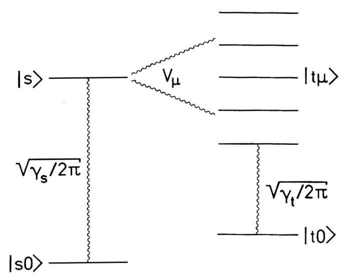

Fig. 1. Anticrossing spectroscopy in molecular physics as an example for the doorway mechanism. Taken from Ref. [4].

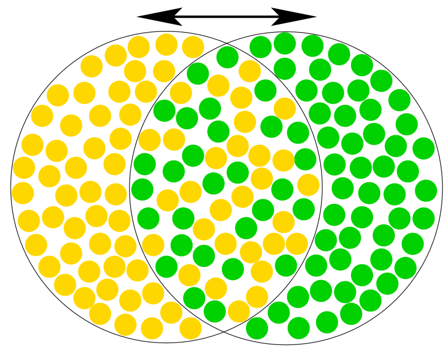

Fig. 3. Linear oscillatory motion of all protons and all neutrons against each others in the giant dipole resonance.

excitations in many-body systems. In the course of doing so, various open questions will be addressed.

The paper is organized as follows. In Sect. 2, the doorway mechanism and its limitations in nuclei are discussed. The microwave experiment is briefly sketched in Sect. 3. In Sect. 4, a statistical model is described. The distribution of the maximum coupling coefficient and comments on its analytical calculation are presented in Sects. 5 and 6, respectively. In Sect. 7, directed spatial correlators are studied. Conclusions are given in Sect. 8.

2. Collective excitations in nuclei

In the cross-sections of electric dipole radiation, a very large peak is seen at higher excitation energies E_x. As Fig. 2 schematically displays, this striking resonance is much larger than all other electric dipole resonances. It is thus referred to as giant dipole resonance (GDR) [1]. It is found in all nuclei, its excitation energy roughly scales as $E_{\rm GDR} \sim A^{-1/3}$ where A is the mass number, that is, the number of nucleons. The giant dipole resonance can be interpreted as a linear oscillatory motion of all protons and all neutrons against each others, as shown in Fig. 3. A simple model is thus obtained by ignoring the relative motion of protons to one another and neutrons to one another. They are viewed as confined in two spheres, one for the protons, one for the neutrons, within which the particles are "frozen", no relative motion occurs. Hence, the effective motion is as collective as possible, it is a one-dimensional linear oscillation of these two spheres against each others. The state constructed in this way, however, is almost certainly no eigenstate of the true many-body Hamiltonian. A true eigenstate will also contain relative motion of the particles within each sphere. The closer the excitation energy to the peak energy, the less relevant is this single particle motion. The further away from the peak energy, the more important is it. The resulting resonance is very broad. The level density is typically so high that the individual nuclear resonances forming this resonance cannot be resolved. The width of the GDR, the spreading width Γ, is thus the only characteristic information. It is a measure for the coupling strength between the simple model for the collective state at energy $E_{\rm GDR}$ to the surrounding background states which are of single-particle type. The true states are then constructed as superpositions of the simple collective state and the background of the single-particle states. As the individual nuclear resonances cannot be resolved anyway, it is reasonable to average over the background states. The simplest observable thereby calculated is the Wigner strength function, that is, the local density of states [1, 2, 8] around the peak position $E_{\rm GDR}$,

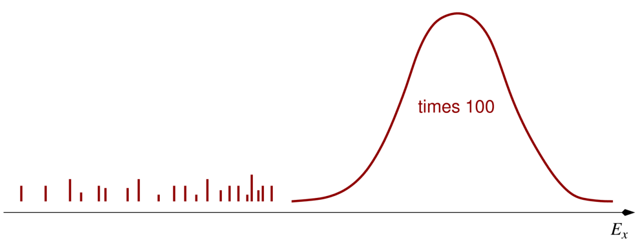

Fig. 2. Schematic drawing of the cross-section for electric dipole radiation in nuclear physics. The big peak to the right is the giant dipole resonance, the small peaks to the left are pygmy resonances.

$$\varrho_{\rm GDR}(E_x) = \frac{1}{\pi}\frac{\Gamma/2}{(E_x - E_{\rm GDR})^2 + \Gamma^2/4}. \tag{1}$$

This Lorentzian shape, also referred to as Breit–Wigner shape, is robust, it is found under very general conditions [1].

From the viewpoint of quantum chaos, it is highly interesting to know whether the level statistics under the GDR is chaotic or not. Obviously, there is no way to address this issue with experimental data due to the lack of resolution. One should emphasize that the Wigner strength function (1) and related measured observables cannot help here, because they are almost insensitive to the level statistics of the background states [1]. But still: there is good reason to assume that the levels under the GDR are chaotic, since the level statistics at these higher excitation energies has been found to be chaotic in the cases where it is experimentally accessible, especially in the compound nuclear resonances, see Ref. [8] and references therein. Hence, the implicit assumption emerged that the doorway mechanism always comes with chaotic statistics of the background states. The analysis [9] of the magnetic analog of the GDR came as a considerable, entirely unexpected surprise: At low excitation energies, deformed nuclei can move just like a pair of scissors. The protons and neutrons in this scissors mode excitation (SME) can be viewed as confined in two ellipsoids which oscillate against each others as displayed in Fig. 4. The corresponding excitation energy scales as $E_{\mathrm{SME}} \sim \delta A^{-1/3}$, where δ measures the deformation. Again, in the simple model, the protons and neutrons are "frozen", resulting in an effectively one--dimensional motion. In the doorway picture one would then expect these states to be coupled to a background of single-particle excitations. Importantly, about ten or so states are found and clearly resolved in the experiments. They can be attributed to the SME by means of experimental information. Collecting data from different nuclei in the rare earth region, the level statistics was analyzed [9] and found to be regular. This is inherently incompatible with a doorway interpretation, since a coupling between doorway and background states is tantamount to the existence of correlations between the true eigenstates. A fully convincing explanation of these findings is still lacking. One is led to the conclusion that all the states belonging to the scissors mode are collective in their own right. An attempt to picture that is made in Fig. 4. Twelve nucleons, say, can be spatially organized in such a way that the enveloping ellipsoids are different. The moments of inertia do not agree, implying that the excitation energies are different as well. Hence, each SME state belongs to a slightly different ellipsoid. In contrast to the GDR the nucleons inside are "frozen", because the available energy is so low.

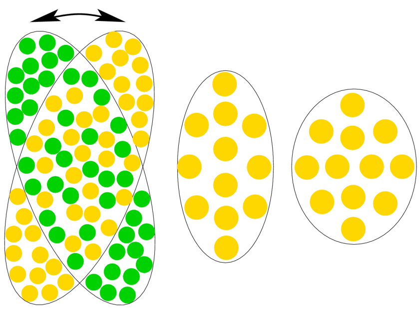

Fig. 4. (left) Rotational oscillatory motion of all protons and all neutrons against each others in the scissors mode. (right) Two ellipses filled with twelve particles without relative motion.

Such an interpretation is corroborated by the experimental and theoretical study on the pygmy resonances (PR) presented in Ref. [10]. The weakly excited PR are found below the GDR as schematically shown in Fig. 2. These excitations may be viewed as a shaking motion of a rigid inner region in the nucleus containing an equal number of protons and neutrons against the excess neutrons in the outer region as displayed in Fig. 5. The

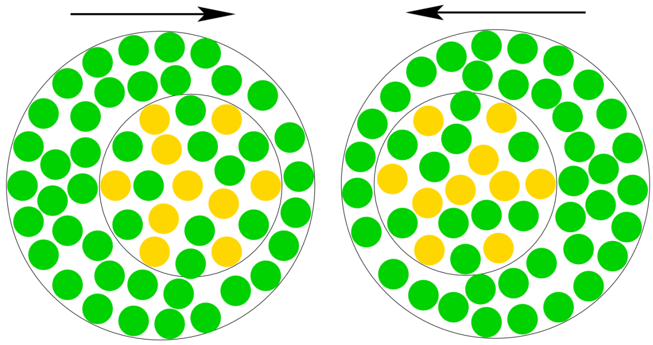

Fig. 5. Pygmy resonances pictured as linear shaking motion of protons and neutrons in the inner region against the excess neutrons in the outer region.

Coulomb interaction only affects the protons, implying that the number of neutrons which the nucleus confines is larger than the number of protons [1]. This neutron excess is the larger the larger the mass number A. The shaking motion comprises regular and chaotic features. In view of the discussion above, one would expect chaotic level statistics with remnants of regularity. Indeed, this is confirmed by the analysis [10]. The complexity of the experimental and the theoretical situation, however, is obstructive of a high statistical significance.

The purpose of this survey over certain aspects of collective motion in nuclei was to show that, first, the doorway picture is a most useful concept in understanding complex systems and that, second, various important questions are still unanswered. In particular, the following topics ought to be addressed:

- Interplay between level statistics and doorway mechanism.
- Structure of wave functions.
- Statistics of observables deriving from the wave functions.

Nuclear experiments are very difficult and often hampered by resolution problems. Wave functions can a priori not directly be measured in traditional quantum systems. The superscars in the barrier billiard, however, provide an ideal object for the study of these issues. This is shown in the sequel. Some of these insights might in turn be useful for many-body physics as well.

3. Superscars in the barrier billiard

Sufficiently flat microwave resonators simulate quantum mechanics in two dimensions [11]. In Ref. [12], the eigenstates and the wave functions of a rectangular microwave billiard with a thin barrier inside were measured, see Fig. 6. The billiard is known to be pseudointegrable [13]. Remarkable states called "superscars", predicted in Ref. [13], were found in addition to many other states of different type [12]. As seen in Fig. 6, the superscars relate to particular classical periodic orbit, more precisely, to families of neutrally stable classical periodic orbits. Ordinary scars [14] are localized around a single unstable periodic orbit. The superscars are thus different, they do not disappear at large quantum numbers. As confirmed in the experiment, they are embedded into a large number of nonscarred wave functions. Importantly, these latter states are of a very different type. As will be discussed in detail, the doorway mechanism applies to these "distinct" superscar states. They act as doorways to the background of the nonscarred wave functions. Four examples of measured superscars are displayed in Fig. 6. The superscars form a family which is confined

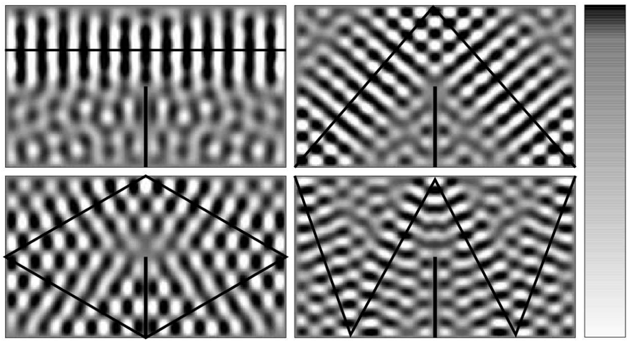

Fig. 6. Examples for measured superscars in the barrier billiard. The concentration along the classical periodic orbits (dashed lines) is clearly visible. Four different families are shown, top row: BB and V, bottom row: D and W. The gray level indicates the value of the wave function (black: highest positive, white: most negative value). Taken from Ref. [7].

to an infinitely long periodic orbit channel (POC) [12]. The amplitude of the scarred wave function tends to zero on the POC boundary. The superscarred wave function may be approximated by a constructed superscar state, defined as an eigenfunction $\Psi_{m,n}^{(\mathrm{F})}(\boldsymbol{r})$ in the infinitely long POC [12, 13]. Here $\mathrm{F} \in \{\mathrm{BB}, \mathrm{V}, \mathrm{D}, \mathrm{W}\}$ labels the superscar families. In the experiment the four families: horizontal bouncing ball BB, inverted V superscars, diamond D and W were measured, see Fig. 6. The indices (m, n) are the numbers of wave maxima along and perpendicular to the POC. Each of the states $\Psi_{m,n}^{(\mathrm{F})}(\boldsymbol{r})$ acts as a doorway to the nonscarred states in the barrier billiard. A measured, that is, true eigenstate $\Psi_{\tilde{f}}(\boldsymbol{r})$ at the properly unfolded [8] frequency $\tilde{f}$ has the overlap

$$c_{m,n} = \langle \Psi_{m,n}^{(\mathrm{F})} | \Psi_{\tilde{f}} \rangle \tag{2}$$

with the constructed superscars [12, 13]. The distribution of these overlaps nicely follows a Breit–Wigner shape [7, 12]. Hence, the superscar strength spreads into the neighboring nonscarred background states. This is an essential prerequisite for a doorway interpretation. In the sequel, a further and much more detailed analysis of the experimental data will be discussed using new observables defined in Ref. [7], namely the distribution of the maximal coupling coefficient and directed spatial correlators.

4. Statistical model

A brief sketch of the statistical model to describe the doorway mechanism [1, 7, 8] is now called for. Eventually, the model employs random matrices, for a review see Ref. [8]. The total Hamiltonian

$$\hat{H} = \hat{H}_s + \hat{H}_b + \hat{V} \tag{3}$$

consists of three parts: $\hat{H}_s$ and $\hat{H}_b$ are the Hamiltonians for doorway and background states, respectively, while the interaction $\hat{V}$ couples these two classes of states. The stationary Schrödinger equations for the uncoupled Hamiltonians are

$$\hat{H}_s|s\rangle = e_s|s\rangle \quad \text{and} \quad \hat{H}_b|b\rangle = e_b|b\rangle. \tag{4}$$

It is assumed that the interaction couples states from different classes only,

$$\langle s|\hat{V}|s'\rangle = \langle b|\hat{V}|b'\rangle = 0 \quad \text{and} \quad \langle b|\hat{V}|s\rangle = v_{bs} \tag{5}$$

for any s, s', b, b'. The constructed superscars, $\Psi_{m,n}^{(\mathrm{F})}(\boldsymbol{r})$ for a given family F but with different (m, n) are the doorway states $|s\rangle$. Obviously, a doorway state is not an eigenstate of the Hamiltonian $\hat{H}$. It is further assumed that the interaction matrix elements, $v_{bs} = v_{sb}$, are Gaussian distributed random variables centered around zero with variance v^2. It has to be stressed that the parameter governing the physics is v/d, where d is the mean level spacing of the background states [1]. This is an often encountered feature of statistical models based on random matrices, see Ref. [8]. In the present case, only a few states carry superscar strength with given values of (m, n). Superscar states with different (m, n) may be viewed as not mixing. Thus, it suffices to consider one single superscar state $|s\rangle$, coupled to N background states $|b\rangle$, where N is large.

The Schrödinger equation for the full Hamiltonian,

$$\hat{H}|n\rangle = E_n|n\rangle \tag{6}$$

can be solved yielding the exact but implicit equation

$$E_n = e_s - \sum_{b=1}^{N} \frac{v_{bs}^2}{e_b - E_n}. \tag{7}$$

The "true" eigenstates are found to be

$$|n\rangle = c_s(n) \left(|s\rangle - \sum_{b=1}^{N} \frac{v_{bs}}{e_b - E_n} |b\rangle \right). \tag{8}$$

Because of normalization, one arrives at the expression

$$c_s(n) = \left[1 + \sum_{b=1}^{N} \frac{v_{bs}^2}{(e_b - E_n)^2} \right]^{-1/2} \tag{9}$$

for the superscar coupling coefficients to each eigenstate.

A random matrix simulation for the coupling coefficients $c_s(n)$ is carried out [7] including $N = 294$ background states. This was the number of nonscarred states found in the experiment. From general considerations, one can imagine three different scenarios for the statistics of the background states. As shown in Fig. 7, the statistics is either regular, that is, Poisson if the levels are uncorrelated, or pseudointegrable, that is, semi–Poisson, or chaotic, that is, Wigner–Dyson. The latter two cases which apply to correlated levels are distinguished by the range of the correlations. Semi-Poisson statistics is found if only neighboring levels interact, and Wigner–Dyson statistics results if all levels are correlated with each other. The barrier billiard is pseudointegrable, and the spacings between the levels are semi-Poisson distributed [15]. Thus a semi-Poisson ensemble of $N + 1$ states is generated [7]. The doorway state is chosen as the middle state, it interacts with the surrounding N states. For each realization, energies and wave functions are numerically calculated, and the overlap between the superscar and the surrounding states is calculated. From these simulations, v/d is extracted for each superscar family. The spreading width is then given by

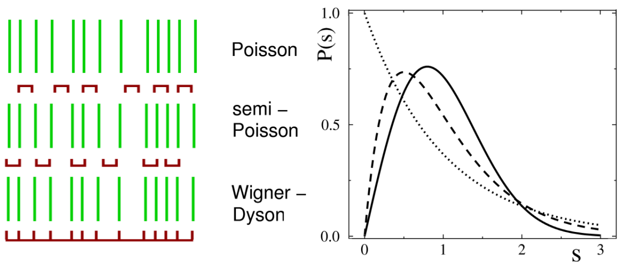

Fig. 7. (left) Different spectral correlations, from top to bottom: no correlations (Poisson), correlations between neighboring levels (semi-Poisson), correlations between all levels (Wigner–Dyson). (right) Nearest neighbor spacing distributions $P(s)$ in this order as dotted, dashed and solid lines, respectively.

$$\Gamma = 2\pi \frac{v^2}{d} \quad \text{or equivalently} \quad \frac{\Gamma}{d} = 2\pi \left(\frac{v}{d}\right)^2 . \tag{10}$$

These relations hold under general circumstances [1, 8].

5. Distribution of the maximum coupling coefficients

The superscar strength $c_s^2(n)$ spreads over the different eigenstates $|n\rangle$ in the form of a Breit–Wigner distribution (1) with spreading width Γ given by Eq. (10). In the barrier billiard, the spreading is over a few states only [12] which means that v/d is smaller than unity. Hence the Breit–Wigner distribution and the spreading width themselves are not well-suited statistical observables.

As a much better measure the maximum coupling coefficients over all states,

$$c_{\max} = \max(|c_{m,n}|) \tag{11}$$

for a given superscar with the overlaps $c_{m,n}$ defined in Eq. (2) are introduced [7]. Importantly, it can be inferred from the experiment. Only a rather small number of states carry strength from the doorway state, that is, from the constructed superscar. The peak of the fitted Breit–Wigner distribution thus tends to deviate from the measured largest superscar strength. Put differently, the discretely measured state is not found exactly at the peak position. One may, however, directly compare the maximum measured value to the corresponding value $\max(c_s(n))$ obtained from the numerical simulations using Eq. (9). It is convenient to consider the squares. Of course, higher moments can be studied as well. It is even possible to study the *full distribution* of these maximum coupling coefficients for a superscar family F. In Ref. [16], the first two moments of the $c_{\max}^2$ distribution were investigated, the underlying assumptions, however, are not valid in the present context. It is a most welcome feature that the shape of the $c_{\max}^2$ distribution strongly depends on the interaction strength v/d. It is also found to be a particularly sensitive measure for small values of v/d, that is, of the order one or smaller.

In Fig. 8 distributions of measured $c_{\max}^2$ are displayed for each superscar family F together with the best fit curves of the random matrix model. The fits yield the

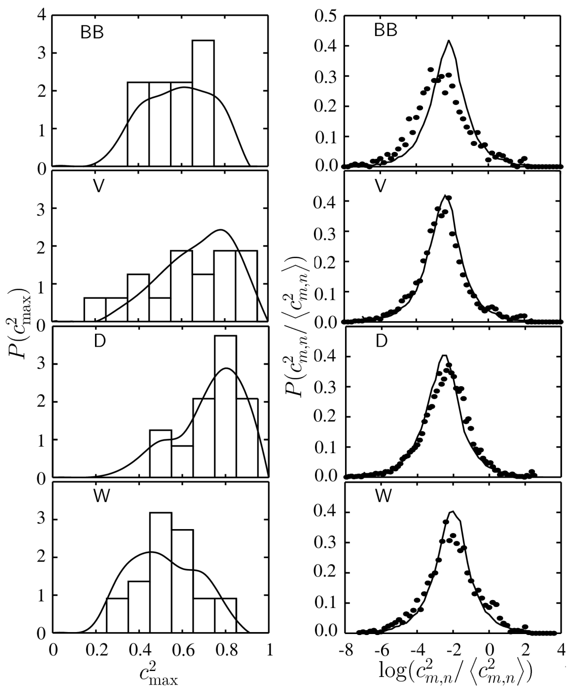

Fig. 8. (left) $c_{\max}^2$ distributions obtained from the experiment (histogram), compared to the fit of the random matrix model predictions (solid line). (right) Normalized distributions of coupling coefficients spread over all states on a logarithmic scale. Experimental distributions (dots) are compared with the random matrix model predictions. Taken from Ref. [7].

following values for the interaction strength: for the BB superscar $v/d = 0.45$, for the V superscar $v/d = 0.35$, for the D superscar $v/d = 0.3$, and for the W superscar $v/d = 0.55$. The interaction strengths are small and thus the Breit–Wigner shape for the doorway strength function is compatible with earlier findings [17]. The V, D, W superscar families comprise 16, 25 and 22 measured states, respectively, while the BB superscar family contains only 9. The fit in this latter case has thus higher uncertainty. The averaged measured and calculated $c^2_{\max}$ values are listed in the Table and discussed in Sect. 8.

It is instructive to also look at the distribution of the coupling coefficients over all eigenstates [7]. The strength of each constructed superscar is measured and calculated over all 294 states. The major part of the strength is concentrated in a few states only. Figure 8 shows measured distributions compared to random matrix simulations for different interaction strengths v/d resulting from the fit to the $c^2_{\max}$ distributions. Obviously, the model reproduces the experimental distributions for all superscar families well except in the case of the BB superscar family because of the small number of superscars. Nevertheless, one also sees that the distribution of the maximum coupling coefficients is the superior observable.

TABLE

Experimental results with standard errors of the mean versus results from the random matrix model (RMT) and directed correlators (Corr) for averaged $c^2_{\max}$ values and spreading width Γ.

F	$\langle c^2_{\max}\rangle$		Γ		
	Exp	RMT	Corr	Exp	RMT
BB	0.58 ± 0.05	0.58	0.81	0.9 ± 0.1	1.3
V	0.63 ± 0.05	0.68	0.69	0.8 ± 0.1	0.8
D	0.74 ± 0.03	0.72	0.69	0.9 ± 0.1	0.6
W	0.54 ± 0.03	0.51	0.49	1.0 ± 0.1	1.9

6. Remarks on the analytical calculation

Only a few general remarks will be made here, because there is a surprising connection to a large number of random matrix models. To analytically calculate the distribution of the maximum overlaps $\max(c_s(n))$, one has to average over the interaction matrix elements and over the Hamiltonian modeling the background states. Denoting this average by square brackets, the seeked distribution is

$$p_{\max}(c) = \langle \delta(c - \max(c_s(n)))\rangle. \tag{12}$$

It is closely related to the distribution of the overlap between the evolved doorway state and the unperturbed doorway state $|0\rangle$, say,

$$p_0(c) = \langle \delta(c - |c_s(0)|)\rangle. \tag{13}$$

Hence, for not too strong an interaction we should have

$$p_{\max}(c) \approx p_0(c). \tag{14}$$

This approximation is certainly good as long as the mean interaction strength is an order of magnitude smaller than the mean level density of the background states. The numerical simulations strongly corroborate this statement. Hence, it suffices to focus on $p_0(c)$, which can be treated analytically. The calculations and the results will be given and discussed elsewhere [18], here only the surprising connection already announced above is addressed.

Let us consider the chaotic case and unitary symmetry. Using supersymmetric techniques, the calculation of $p_0(c)$ for finite level number N is found to be equivalent to the evaluation of an integral over two *ordinary* 2×2 Hermitean matrices σ and τ,

$$\int \mathrm{d}[\sigma] \exp\left(-\mathrm{tr}\sigma^2\right) \int \mathrm{d}[\tau] \exp\left(-\mathrm{tr}\tau^2\right) \times \det{}^{N-1}\left[\sigma + g(v^2)\tau\right] \det\tau, \tag{15}$$

where the function $g(v^2)$ contains all information about the interaction strength v.

Two-matrix models of related form appear remarkably often when a random matrix model is mapped onto a model in a dual matrix space by means of a Hubbard–Stratonovich transformation [8]. One is tempted to speculate that there is a deeper reason for this frequent occurrence which is not yet understood.

7. Directed spatial correlators

In traditional quantum systems, the wave functions as such are not experimentally accessible. One can only measure derived quantities such as transition matrix elements. In microwave billiards, however, wave functions can be measured. In the barrier billiard, a large number was obtained [12], which allows one to analyze their statistical properties. As a new observable, directed spatial correlations of the wave functions were introduced in Ref. [7]. Berry [19] considered the correlator

$$C(kr) = \frac{\langle \psi_k(\boldsymbol{R} - \boldsymbol{r}/2)\psi^*_k(\boldsymbol{R} + \boldsymbol{r}/2)\rangle}{\langle |\psi_k(\boldsymbol{R})|^2\rangle} \tag{16}$$

of the wave functions $\psi_k(\boldsymbol{r})$. The average is performed *isotropically* over all vectors $\boldsymbol{R}$ and, for fixed moduli of wave vector $\boldsymbol{k}$ and r, also over all directions of the vector $\boldsymbol{r}$. In the barrier billiard, all wave functions are real, complex conjugation is not needed in Eq. (16). Berry argued that the spatial correlations of a wave function in an ergodic system should coincide with those generated by superimposing plane waves. In two dimensions, the universal prediction $C(kr) = J_0(kr)$ follows, if possible boundary effects are ignored. Here J_0 is the Bessel function of order zero. This behavior was confirmed in a large number of systems [8, 11, 20, 21].

However, the superscars are certainly non-ergodic. Hence, especially tailored observables, the *directed* correlators, were defined in Ref. [7]. Instead of averaging isotropically as for $C(kr)$, one averages either only across or only along the channel in which the superscar exists, similar to Ref. [22]. The resulting correlators are $C^{\perp}(kr)$ and $C^{||}(kr)$, respectively. In the top row of Fig. 9 the

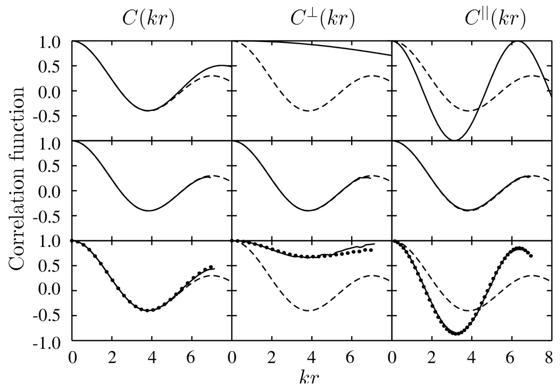

Fig. 9. Wave function correlators, the $J_0(kr)$ prediction is always given as dashed line. Top row: correlators of the constructed V superscar state as solid lines: the isotropic $C(kr)$ as well as the directed $C^{\perp}(kr)$ and $C^{||}(kr)$. Middle row: the same observables are depicted as solid lines for the averages over all experimental wave functions in the barrier billiard. Bottom row: the correlators averaged over all observed V superscars are shown as solid lines and the correlators resulting from Eq. (17) with $c^2_{\max} = 0.69$ are shown as filled circles. Taken from Ref. [7].

three correlators of a constructed V superscar $\Psi^{(\mathrm{V})}_{m,n}(\boldsymbol{r})$ are displayed. The isotropic correlator $C(kr)$ agrees with the $J_0(kr)$ prediction up to a certain scale, but the directed correlators strongly deviate from it. The results for $C^{\perp}(kr)$ and $C^{||}(kr)$ show that the constructed superscar fills the channel and moves through it as a sine wave. This is already seen in Fig. 6. The information about the form of the waves, however, is washed out when averaging over all wave functions in the billiard. As the middle row of Fig. 9 shows, each of the three correlators obtained for all measured wave functions coincides with the $J_0(kr)$ prediction for chaotic systems. Hence, one may use Berry's random wave approach even though our billiard system is pseudointegrable. Importantly only the two-point correlations are used [7] up to $kr = 8$. At larger scales, deviations due to pseudointegrability would manifest themselves.

These observations yield information about the superscar coupling coefficients. Correlators averaged over all experimentally observed V superscars are displayed in the bottom row of Fig. 9. They are similar to, but slightly different from those for the constructed V superscars in the top row. The difference is due to the leaking of the superscar out of the channel or, in the language of the doorway description, due to the coupling of the background states to the superscar. This makes it possible [7] to model the measured superscars $\Psi^{(\mathrm{F})}_{\tilde f}(\boldsymbol{r})$ for family F as a linear combination of a constructed superscar $\Psi^{(\mathrm{F})}_{m,n}(\boldsymbol{r})$, which only contributes in the channel, and a state $\widetilde{\chi}_k(\boldsymbol{r})$ which is ergodically distributed everywhere in the billiard. Hence one has

$$\Psi^{(\mathrm{F})}_{\tilde f}(\boldsymbol{r}) = c_{\max}\, \Psi^{(\mathrm{F})}_{m,n}(\boldsymbol{r}) + \sqrt{1 - c^2_{\max}}\,\widetilde{\chi}_k(\boldsymbol{r}). \qquad (17)$$

This ansatz takes up the random matrix model above and extends it by also modeling the spatial dependence. The states describing the background should, first, have $J_0(kr)$ correlations and, second, be orthogonal to $\Psi^{(\mathrm{F})}_{m,n}(\boldsymbol{r})$. These requirements can be met by choosing the "scarless" plane waves

$$\widetilde{\chi}_k(\boldsymbol{r}) = \frac{\chi_k(\boldsymbol{r}) - \langle\, \Psi^{(\mathrm{F})}_{m,n}|\chi_k\rangle\, \Psi^{(\mathrm{F})}_{m,n}(\boldsymbol{r})}{\sqrt{1 - \langle\, \Psi^{(\mathrm{F})}_{m,n}|\chi_k\rangle^2}} \qquad (18)$$

with standard plane waves $\chi_k(\boldsymbol{r})$. The superscar contribution in the plane waves is small, but it is not negligible; the distribution of the overlaps $\langle\, \Psi^{(\mathrm{F})}_{m,n}|\chi_k\rangle$ has a standard deviation of 0.13. It was checked [7] that the correlator of the $\widetilde{\chi}_k(\boldsymbol{r})$ follows the $J_0(kr)$ prediction very closely. The three correlators for the model (17) were worked out. They depend on $c_{\max}$ which is, just as in the random matrix model above, the maximum coupling coefficient to the superscar doorway. Fits to the measured superscar families yield the coupling coefficients $c_{\max}$. The fits for the V superscar are shown in Fig. 9. The resulting $\langle c^2_{\max}\rangle$ values are listed in the Table and discussed in Sect. 8.

8. Conclusions

The results of the data analysis are compiled in the Table. The distribution of the maximum coupling coefficient and the directed correlators yield results which agree well. This strengthens the line of reasoning followed above. For comparison, the resulting Γ values are also given in the Table. Obviously, the new observables are more appropriate which is born out in the large standard deviation of the Γ distribution which is, for example for the W superscar family, 0.8. The doorway interpretation yields an in-depth understanding of the experimental findings. Both new observables considerably improve the insight into the statistical features of the doorway mechanism. It is important and encouraging that the two analyses agree.

It would be a major effort to carry out such a study for data obtained from realistic nuclear structure calculations. Nevertheless, even though an experimental analysis of these issues is out of question for nuclei, such a study of nuclear structure calculations would be highly rewarding. It would yield a much improved understanding of how the doorway mechanism emerges from the dynamics of the many-body system. In particular, the most important result would be an understanding of how the doorway mechanism ceases to work when approaching the region near the ground state with low level density — as is the case for the scissors mode. This in turn would shed new light on aspects of collective motion which are at present only poorly understood.

Acknowledgments

I thank my collaborators of Refs. [7, 9, 10]. Discussions with E. Bogomolny and B. Dietz were highly valuable. I acknowledge support from Deutsche Forschungsgemeinschaft within Sonderforschungsbereich SFB/TR12.

References

[1] A. Bohr, B. Mottelson, *Nuclear Structure*, Vol. 1, W.A. Benjamin, Reading (Massachusetts) 1969.

[2] V. Zelevinsky, *Ann. Rev. Nucl. Part. Sci.* **46**, 237 (1996).

[3] V.V. Sokolov, V. Zelevinsky, *Phys. Rev. C* **56**, 311 (1997).

[4] T. Guhr, H.A. Weidenmüller, *Chem. Phys.* **146**, 21 (1990).

[5] I. Kawata, H. Kono, Y. Fujimura, A.D. Bandrauk, *Phys. Rev. A* **62**, 031401(R) (2000).

[6] M.S. Hussein, V. Kharchenko, L.F. Canto, R. Donangelo, *Ann. Phys.* **284**, 178 (2000).

[7] S. Åberg, T. Guhr, M. Miski-Oglu, A. Richter, *Phys. Rev. Lett.* **100**, 204101 (2008).

[8] T. Guhr, A. Müller-Groeling, H.A. Weidenmüller, *Phys. Rep.* **299**, 189 (1998).

[9] J. Enders, T. Guhr, N. Huxel, P. von Neumann-Cosel, C. Rangacharyulu, A. Richter, *Phys. Lett. B* **486**, 273 (2000).

[10] J. Enders, T. Guhr, A. Heine, P. von Neumann--Cosel, V.Y. Ponomarev, A. Richter, J. Wambach, *Nucl. Phys. A* **741**, 3 (2004).

[11] H.-J. Stöckmann, *Quantum Chaos: An Introduction*, Cambridge University Press, Cambridge 2000.

[12] E. Bogomolny, B. Dietz, T. Friedrich, M. Miski-Oglu, A. Richter, F. Schäfer, C. Schmit, *Phys. Rev. Lett.* **97**, 254102 (2006).

[13] E. Bogomolny, C. Schmit, *Phys. Rev. Lett.* **92**, 244102 (2004).

[14] E.J. Heller, *Phys. Rev. Lett.* **53**, 1515 (1984).

[15] E.B. Bogomolny, U. Gerland, C. Schmit, *Phys. Rev. E* **59**, R1315 (1999).

[16] E. Vergini, *J. Phys. A* **37**, 6507 (2004).

[17] N. Frazier, B.A. Brown, V. Zelevinsky, *Phys. Rev. C* **54**, 1665 (1996).

[18] H. Kohler, T. Guhr, S. Åberg, in preparation.

[19] M.V. Berry, *J. Phys. A* **10**, 2083 (1977).

[20] V. Doya, O. Legrand, F. Mortessagne, C. Miniatura, *Phys. Rev. E* **65**, 056223 (2002).

[21] K. Schaadt, T. Guhr, C. Ellegaard, M. Oxborrow, *Phys. Rev. E* **68**, 036205 (2003).

[22] A. Bäcker, R. Schubert, *J. Phys. A* **35**, 539 (2002).